AD-A232 438

(2)

REPORT DOCUMENTATION PAGE

Form Approved
OMB No. 0704-0188

1. Agency Use Only *(Leave blank).*	2. Report Date. 1990	3. Report Type and Dates Covered. Journal Article

4. Title and Subtitle.

In Situ Porosity and Permeability of Selected Carbonate Sediment: Great Bahama Bank Part 1: Measurements

5. Funding Numbers.

Program Element No. 61153N
Project No 03205
Task No. 330
Accession No DN257003

6. Author(s).

Richard H. Bennett, Huon Li, Douglas N. Lambert, Kathleen M. Fischer, Donald J. Walter, Charles E. Hickox, Matthew H. Hurlbert, Tokuo Yamamoto, and Mohsen Badiey

7. Performing Organization Name(s) and Address(es).

Naval Oceanographic and Atmospheric Research Laboratory
Ocean Science Directorate
Stennis Space Center, MS 39529-5004

8. Performing Organization Report Number.

JA 360:018:89

9. Sponsoring/Monitoring Agency Name(s) and Address(es).

Naval Oceanographic and Atmospheric Research Laboratory
Ocean Science Directorate
Stennis Space Center, MS 39529-5004

10. Sponsoring/Monitoring Agency Report Number.

JA 360:018:89

11. Supplementary Notes.

MG

12a. Distribution/Availability Statement.

Approved for public release; distribution is unlimited.

12b. Distribution Code.

13. Abstract *(Maximum 200 words).*

In situ porosity and permeability were measured on Great Bahama Bank sediments using electrical conductivity and permeability probes. Core samples were recovered at the probe measurement sites for laboratory determinations of porosity and permeability. Penetration depths of cores and probes were approximately 2.5 m subbottom.

In situ porosities of the oolitic sands for depths of 0-2.5 m subbottom ranged between 36% and 50%, and at sites in the somewhat muddier oolitic sediments the porosities ranged from 42% to 61%. The in situ permeabilities ranged from 0.0032 cm/s (3.3 darcys) to 0.068 cm/s (71 darcys) at the sites where porosities were determined. Laboratory values of porosity are comparable to values obtained by in situ measurements; however, laboratory permeability values are approximately an order of magnitude lower than in situ values. The reduced permeability measured in the laboratory is attributed to disturbance of the microfabric during coring, transport, and laboratory sampling. A detailed examination of the microfabric can be found in a companion article (Bennett et al. 1990)

The high in situ porosities and permeabilities of these carbonate sediments are predominantly the result of the combined effects of both the sediment grain size distribution and the microfabric. The classification scheme of Dunham (1962) for carbonate rocks (wackestone, packstone, etc.) does not always provide a clear picture of some of the crucial properties of carbonate sediments (porosity, permeability, etc.), nor does this scheme provide a realistic functional description of the behavior of these sediments when subjected to static and dynamic stresses.

14. Subject Terms.	15. Number of Pages.
(U) Sediment Transport; (U) Sediments; (U) Pore Pressure; (U) Clay	28
	16. Price Code.

17. Security Classification of Report.	18. Security Classification of This Page.	19. Security Classification of Abstract.	20. Limitation of Abstract.
Unclassified	Unclassified	Unclassified	SAR

Marine Geotechnology, Volume 9, pp. 1–28
Printed in the UK. All rights reserved

0360-8867/90 $3.00 + .00

In Situ Porosity and Permeability of Selected Carbonate Sediment: Great Bahama Bank Part 1: Measurements

RICHARD H. BENNETT
HUON LI
DOUGLAS N. LAMBERT
KATHLEEN M. FISCHER
DONALD J. WALTER

Seafloor Geosciences Division
Naval Oceanographic and Atmospheric Research Laboratory
John C. Stennis Space Center, MS 39529

CHARLES E. HICKOX

Sandia National Laboratories
Albuquerque, NM 87185

MATTHEW H. HULBERT

Pittman-Moore, Inc.
Terre Haute, IN 47808

TOKUO YAMAMOTO
MOHSEN BADIEY

Geo-Acoustics Laboratory
Rosenstiel School of Marine and Atmospheric Science
Division of Applied Physics and Ocean Engineering
University of Miami
Miami, FL 33149

Abstract *In situ porosity and permeability were measured on Great Bahama Bank sediments using electrical conductivity and permeability probes. Core samples were recovered at the probe measurement sites for laboratory determinations of porosity and permeability. Penetration depths of cores and probes were approximately 2.5 m subbottom.*

In situ porosities of the oölitic sands for depths of 0–2.5 m subbottom ranged between 36% and 50%, and at sites in the somewhat muddier oölitic sediments the porosities ranged from 42% to 61%. The in situ permeabilities ranged from 0.0032 cm/s (3.3 darcys) to 0.068 cm/s (71 darcys) at the sites where porosities were determined. Laboratory values of porosity are comparable to values obtained by in situ measurements; however, laboratory permeability values are approximately an order of magnitude lower than in situ values. The reduced permeability measured in the laboratory is attributed to disturbance of the microfabric during coring.

Mohsen Badiey's present affiliation is the University of Delaware.

transport, and laboratory sampling. A detailed examination of the microfabric can be found in a companion article (Bennett et al. 1990).

The high in situ porosities and permeabilities of these carbonate sediments are predominantly the result of the combined effects of both the sediment grain size distribution and the microfabric. The classification scheme of Dunham (1962) for carbonate rocks (wackestone, packstone, etc.) does not always provide a clear picture of some of the crucial properties of carbonate sediments (porosity, permeability, etc.), nor does this scheme provide a realistic functional description of the behavior of these sediments when subjected to static and dynamic stresses.

Keywords sediments, marine, porosity, permeability, Great Bahama Bank, in situ, laboratory, carbonate

Introduction

Holocene carbonate sediments of the Bahamas and South Florida coastal areas have been studied extensively during the past few decades. Investigations have addressed numerous aspects of shallow-water carbonate sedimentation in order to understand the various geological, biological, and chemical processes and factors responsible for the formation, modes of deposition, depositional environments, diagenesis, and physical properties of these deposits (Illing 1954; Ginsburg et al. 1963; Purdy 1963a, 1963b; Shinn et al. 1969; Morelock and Bryant 1972; Mullins and Neumann 1979). More recently, studies have focused on carbonate sediment and rock porosity, permeability, and fabric because of the importance of these properties to the processes of consolidation/compaction (dewatering), diagenesis, cementation, and hydrocarbon accumulation (Enos and Sawatsky 1981; Bhattacharyya and Friedman 1984; Schmoker and Hester 1986; Evans and Ginsburg 1987).

The depositional microstructure and mass physical properties of both carbonate and terrigenous sediments play critical roles in determining postdepositional properties during burial diagenesis and consolidation processes (Bennett and Nelsen 1983; Bennett and Hulbert 1986). A serious lack of reliable geological information and geotechnical data exists for the depositional properties of sediments because of the difficulty in obtaining undisturbed samples and the previous lack of adequate technology to measure the required properties at and near the sediment-water interface, i.e., within the upper few centimeters. Indeed, the measurement of physical properties of surficial (upper few meters), noncohesive sediments is a formidable task and accounts, in large part, for the deficiency of data for many important properties (mechanical, physical, geoacoustic, etc.).

The purpose of this investigation was to determine in situ physical properties of selected surficial carbonate sediments and to evaluate the lateral and vertical variability of these properties over a limited scale. Another objective was to establish a reliable data set of critical sediment properties of carbonate sands for geoacoustic modeling, seafloor stability analysis, and other relevant U.S. Navy applications. The significance and role of the microfabric in determining the physical properties of the sediment also were investigated (Bennett et al. 1990).

Study of the physical and mechanical properties of surficial sediments provides data not only for applied work but also provides a basis for gaining insight into the behavior of deposits under static and dynamic stresses and the depositional and sediment transport processes characteristic of geological environments (Li and Bennett, in press). An understanding of the sediment properties at the sediment-water interface gives the "end

member" characterization of the "initial" state of the material for evaluating postdepositional processes of consolidation (dewatering) and diagenesis.

The Great Bahama Bank was selected for the field measurements because of the following factors: (1) sediment types available (oölites) are texturally less complex than many other shallow-water carbonates; (2) the sediments are located relatively close to shore-based laboratories; (3) this region has been relatively well studied geologically; (4) in situ measurements and sampling were logistically simple in the shallow waters of this region; and (5) the sites were shallow enough for sufficient transfer of wave energy to the bottom sediments to permit bottom shear modulus measurements which were part of the field program (Yamamoto and Bennett 1986; Connor 1986).

The Andros Platform of the Great Bahama Bank is a shallow water site of carbonate deposition. The surface sediments of this region have been differentiated into five major facies based on volume percentages of particle types larger than 1/8 mm and weight percentage of particles smaller than 1/8 mm (Imbrie and Purdy 1962; Purdy 1963a, 1963b). The five major facies are (1) coralgal, (2) grapestone, (3) oölitic, (4) oölite, and (5) lime mud. Sedimentological descriptions of these facies and the environments of deposition have been studied in detail by Purdy (1963a, 1963b), and further discussion of these aspects is beyond the scope of this article. Four sites were selected on the Great Bahama Bank (Fig. 1) in water depths of 3.5 to 4 m. The four sites were located in the general areas defined by Imbrie and Purdy (1962) as pellet mud (a subfacies of the lime mud facies) and the oölitic facies. The lateral extent of the pellet mud subfacies near sites 3 and 4 of this study was defined by Imbrie and Purdy (1962) on the basis of only one sediment sample, and thus the boundary or lateral extent of the deposit was poorly constrained. In our samples, the sand-size particles which survived gentle wet sieving were predominantly ellipsoidal in shape and quite hard. Examination of sediments by light and electron microscopy revealed that the sand-size particles are oöids. The oöid nuclei are composed of either various types of carbonate fragments or indurated fecal pellets (samples examined by R. Rezak, personal communication 1989). The nuclei are coated with densely packed aragonite needles arranged tangentially to the surface of the particles which, for practical purposes, fit the classical definition of oölitic particles (Ginsburg et al. 1963).

Site Surveys, Instrumentation, and Techniques

Specific field sites were selected by analysis of grab samples and subbottom profiles during a rapid survey in the areas of interest. A Honeywell ELAC 15-kHz subbottom acoustic profiler (sediment classifier) was used for the survey to compare the acoustic properties of the areas of interest. Four sites were selected: Sites 1 and 2 were oölitic sands with a small fraction of fines (less than 62 μm); sites 3 and 4 were muddy (silty) oölitic sands. The 15-kHz profiles of the two areas are very similar acoustically, and both areas show sediment thicknesses of about 2.5 to 3 m (Fig. 2). Profiles over the oölitic sand show a distinct reflector, at about 1.5 m subbottom (below which the porosity decreases significantly), which is partially visible in the profiles of the muddy oölitic sands. The 15-kHz acoustic profiles of the muddy oölite are somewhat more diffuse than those of the sandy area of sites 1 and 2. The major difference in the two sites was the higher percentage of fines present at sites 3 and 4. Water depths were only slightly greater (0.5 m or less) at sites 1 and 2.

Large diameter (7.9-cm ID, 8.9-cm OD) vibrocores were collected and in situ

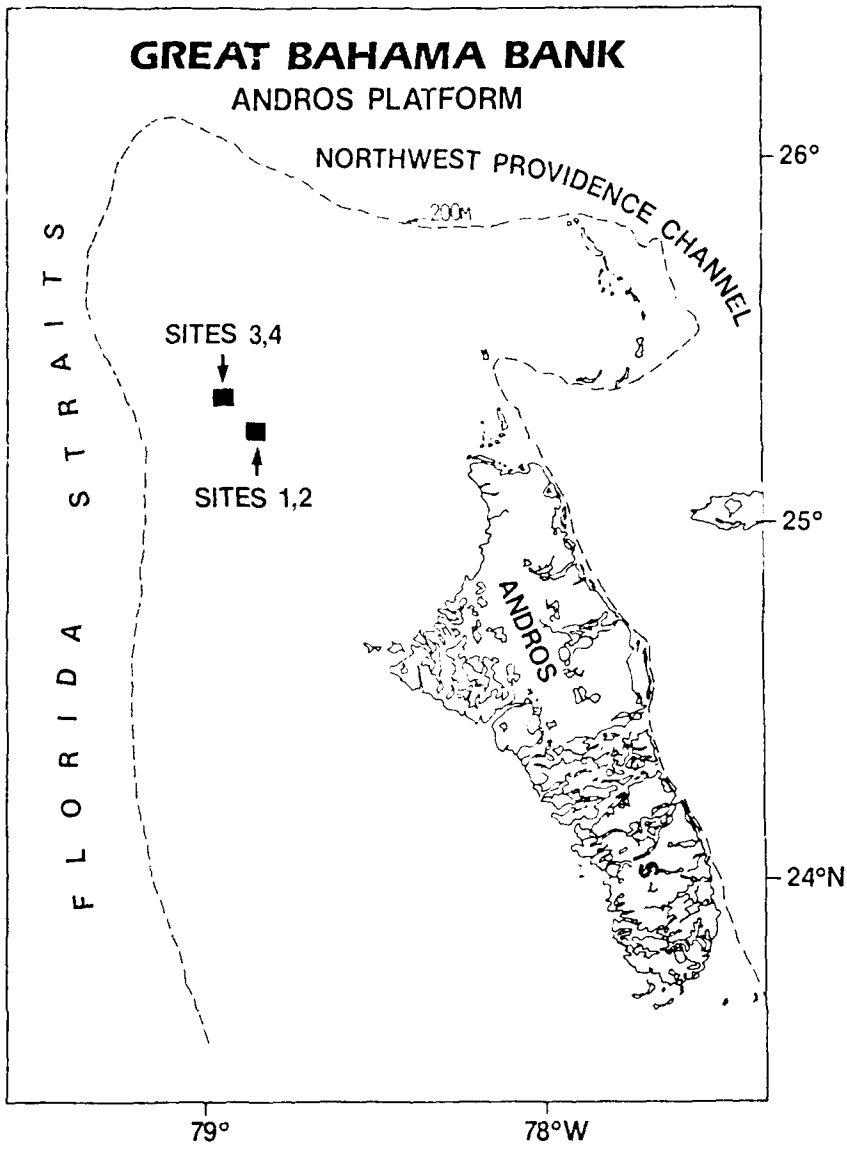

Figure 1. Map of Great Bahama Bank showing locations of sites 1–4.

measurements were conducted at the four sites. Sample locations and penetration depths are summarized in Table 1. The core tubes and conductivity and permeameter probes were attached individually to the vibrocorer frame and driven with a pneumatic head charged by an air compressor (345–689 kPa) located on deck. Core tubes were driven to refusal depths, whereas the in situ probes were driven to selected subbottom depths for determination of permeability and porosity.

The in situ porosity and permeability and laboratory permeability techniques are described in Appendixes A, B, and C. Short, whole-core samples were cut immediately from long vibrocores upon core retrieval in the field. These samples were refrigerated to preserve sample quality for laboratory testing of permeability and porosity and subsam-

pling for microfabric analysis (Bennett et al. 1990). Selected samples were used for the determination of shear modulus and frame loss (Badiey et al. 1988).

Laboratory porosity and grain size distribution were determined by standard techniques (Lambe 1951; Richards 1962). Numerous subsamples of cores from sites 1 through 4 were carefully wet sieved through a No. 230 mesh (62.5 μm) sieve to separate sands from fines, and the grain size distribution of the fine fraction was determined further by pipette analysis. Average grain densities, which were determined using a helium gas pyconometer, and in situ porosities were used to calculate water content (percent dry weight) and saturated wet bulk density using the following relationships:

$$W\ \% = \frac{100(n\gamma_{sw})}{(1 - n)\gamma_s} \tag{1}$$

and

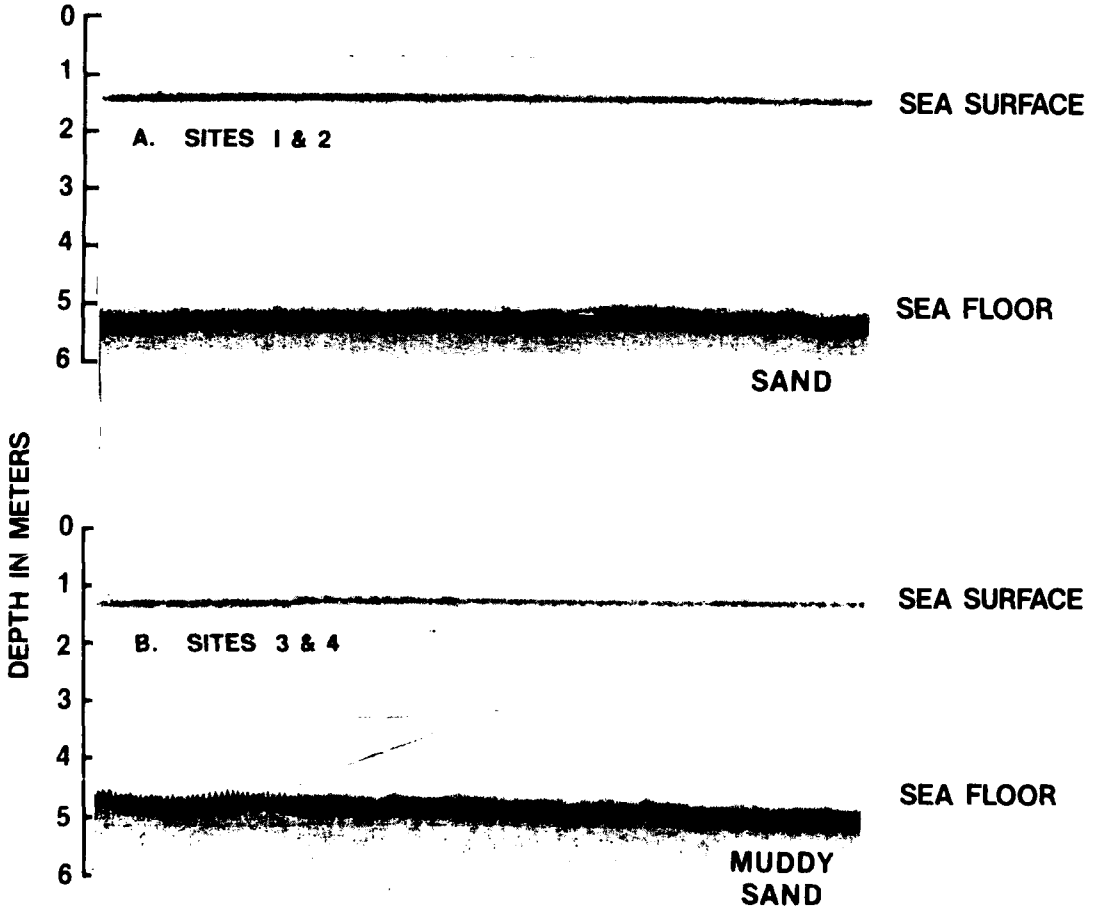

Figure 2. High-resolution-15 kHz acoustic profiles: (*a*) sites 1 and 2; (*b*) sites 3 and 4.

Table 1
Coring and in Situ Measurements, Great Bahama Bank

Site Number	Core Number	Latitude	Longitude	Sample Type	Penetration (m)
1	1A	25°15.8′	78°50.5′	Vibrocore	0.9
1	1A	25°15.8′	78°50.5′	Conductivity	—
1	1A	25°15.8′	78°50.5′	Permeameter	—
1	1B	25°15.8′	78°50.5′	Vibrocore	2.3
2	2A	25°15.9′	78°50.4′	Vibrocore	2.4
2	2A	25°15.9′	78°50.4′	Conductivity	—
2	2A	25°15.9′	78°50.4′	Permeameter	—
3	3A	25°22.2′	78°56.4′	Vibrocore	1.2
3	3A	25°22.2′	78°56.4′	Conductivity	—
3	3A	25°22.2′	78°56.4′	Permeameter	—
3	3B	25°22.2′	78°56.4′	Vibrocore	2.4
3	3C	25°22.2′	78°56.4′	Vibrocore	2.7
4	4A	25°22.2′	78°56.3′	Vibrocore	2.6
4	4A	25°22.2′	78°56.3′	Conductivity	—

$$\gamma_t = (n\gamma_{sw}) + (1 - n)\gamma_s \quad (2)$$

where W = water content expressed as percent dry weight
n = porosity expressed as a decimal, not a percentage
γ_{sw} = density of sea water (1.024 Mg/m^3)
γ_t = saturated wet bulk density or wet unit weight
γ_s = average grain density of the solids

Results

The sediments are classified (Fig. 3) as sand (sites 1 and 2) and silty sand (sites 3 and 4) and are composed predominantly of oölitic grains (>62.5 μm) supported by an aragonitic matrix of silt-size and clay-size particles. Most of the oöids are medium to fine sand size (100–500 μm). The presence of fines creates a slightly cohesive and very porous material. The percentage of fines decreases significantly with burial depth, i.e., with increasing age (Fig. 4). The classification scheme of Dunham (1962) for carbonate rocks, when applied in a limited sense to carbonate sediments, points out the important distinction between a grain-supported material (packstone) and a matrix-supported material (wackestone). Enos and Sawatsky (1981) used Dunham's classification scheme for their study of the Great Bahama Bank sediments. According to Dunham's classification, the sediments investigated during this study are predominantly "wackestones" (matrix supported) based on grain size distribution and porosity, as discussed below. The microfabric examined by scanning electron microscopy (Bennett et al. 1990) also supports the classification of these sediments as wackestones." It should be noted, however, that the carbonates of the present study and those examined by Enos and Sawatsky are not

lithified, and in both studies 62.5 μm is used as the division between grains and fines, rather than 20 μm as used by Dunham.

The in situ porosities (Table 2) for sites 1–4 are plotted as a function of depth of burial in Figure 5. Porosities are somewhat higher and decrease with depth more dramatically at sites 3 and 4 (range n = 61–42%; $n \approx 30\%$ for rock tested at site 3A) compared to sites 1 and 2 (range n = 50–36%). The porosity of the upper 1 m averages 45% at sites 1 and 2 but is considerably higher, 58%, at sites 3 and 4. The porosities at sites 1 and 2 are comparable to the initial (depositional) porosities estimated for the oölitic Miami limestone of the lower Florida Keys (Schmoker and Hester 1986).

The porosities for sediments at sites 1–4 are much higher than are characteristic of clean sandy sediments, but the values are reasonable because of the presence of even a small amount of fines. As pointed out by Enos and Sawatsky (1981), if the large grains (oöids) are in contact, i.e., the sediment is classified as a "packstone," then the addition of fines would result in the filling of intergranular pore space and a reduction in porosity. Porosity would continue to decrease as more fines are added. At the point when all intergranular pore space is completely filled with matrix of a given porosity, further addition of fines results in a matrix-supported sediment and increased porosity. This conceptual model assumes that grain packing remains constant while intergranular pore space is being filled with matrix material of an assumed porosity. In situ porosities versus percent fines are plotted together with data from Enos and Sawatsky (1981) (Fig. 6). It should be noted that for a given porosity the percentage of fines is slightly higher in samples from the present study compared to data from Enos and Sawatsky (possibly indicating a denser grain packing of 0% fines for the sediments of the present study), but the relationship of increasing percentage of fines with increasing porosity is similar. The data by Enos and Sawatsky is best fitted by regression to a third-order polynomial with suggests that for a $\pm$10–15% difference in the percentage of fines, the porosity varies approximately $\pm$15%. This topic is discussed further in a companion article (Bennett et al. 1990).

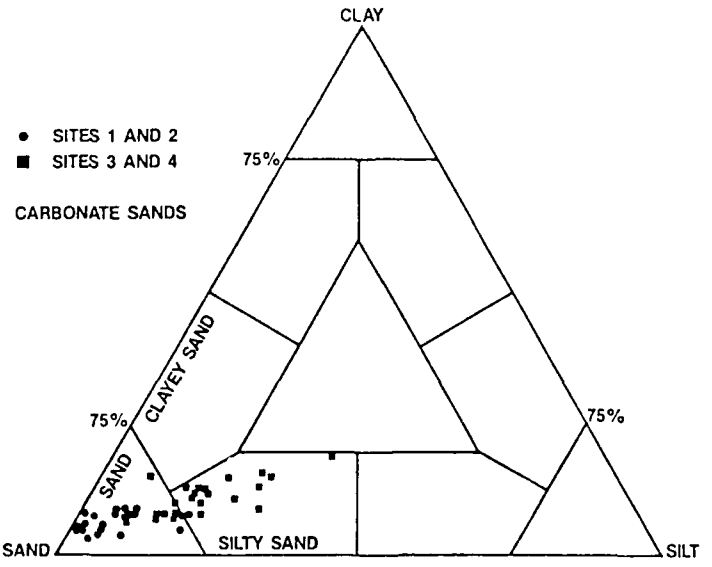

Figure 3. Ternary diagram of grain size distribution: sand, greater than 62.5 μm; silt, 62.5–2 μm; clay, less than 2 μm.

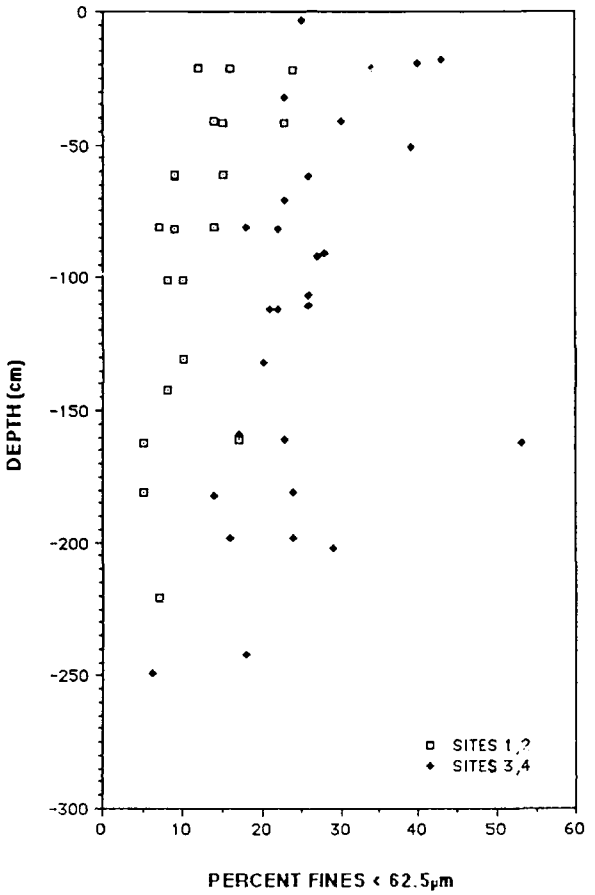

Figure 4. Percent fines (particles less than 62.5 μm) versus depth in core, sites 1–4.

Porosity and permeability were measured in the laboratory on selected samples from sites 1 and 3 and on Ottawa sand (a control sample). Sample descriptions and grain size distributions are given in Table 3. The porosities measured in the laboratory (Table 4) are within the range of values measured by in situ techniques (Table 2). Differences in porosity before and after permeability testing are probably a function of changes brought about by pressurization of the samples to 689 kPa, e.g., resaturation, and by slight variability in the properties of the subsamples tested. The permeabilities measured in the laboratory (Table 4), about one order of magnitude lower than the in situ measurements (Table 5), are low most likely because of sample disturbance during coring, transport, and laboratory testing. In support of this explanation, an additional permeability reduction of two orders of magnitude (to a value for K of 1.99×10^{-2} darcy) was measured on a remodeled sample from site 3 (Table 4). Remodeling produces mechanical disturbance that is severe compared to the disturbance observed in "high-quality" core samples. The reduction in permeability following remolding occurred despite the addition of water to the sample, which increased the porosity from 54% to 62% (Table 4). This decrease in permeability is probably due to a destruction of the large and continuous pathways in the "undisturbed" samples that permit rapid drainage of water through the material.

The laboratory and in situ porosities plotted versus permeabilities (Fig. 7) show a

very wide range of values which is largely a function of the combined effects of grain size distribution and microfabric. Similar observations of the importance of microfabric and grain size distribution to porosity and permeability were found in a study of terrigenous clays, carbonate oozes, and aragonite sands (Bennett et al. 1989). Typically, clean sands display moderate porosities and high-to-moderate permeabilities (Lambe and

Table 2
In Situ Porosity, Great Bahama Bank

Summary	Depth (ft)	Depth (cm)	Formation Factor (F)	Porosity from Resistivity (n)
Site 1	1	30	3.07	45
	2	61	3.47	40
	3	91	2.92	47
	4	122	2.72	50
	5	152	2.90	47
	6	183	2.82	48
	6.2	191	2.96	46
Site 2A	2	61	3.36	41
	2.5	76	3.02	46
	3	91	3.22	43
Site 2B	3	91	3.12	44
	4.8	145	3.04	45
	5	152	2.77	49
	6.2	191	3.46	40
	6.8	206	3.53	40
	7.8	236	3.50	40
	8.2	251	3.85	36
Site 3A	2.8	84	2.87	55
	8.8	267	5.50 (rock)	30
Site 3B	1	30	2.55	61
	2.3	69	2.73	57
	3.2	99	2.77	57
	4	122	2.99	53
	5.2	160	3.11	51
	6.2	191	3.01	52
	7	213	3.23	49
	7.2	221	3.79	42
Site 4	1	30	2.73	57
	7	213	3.27	49

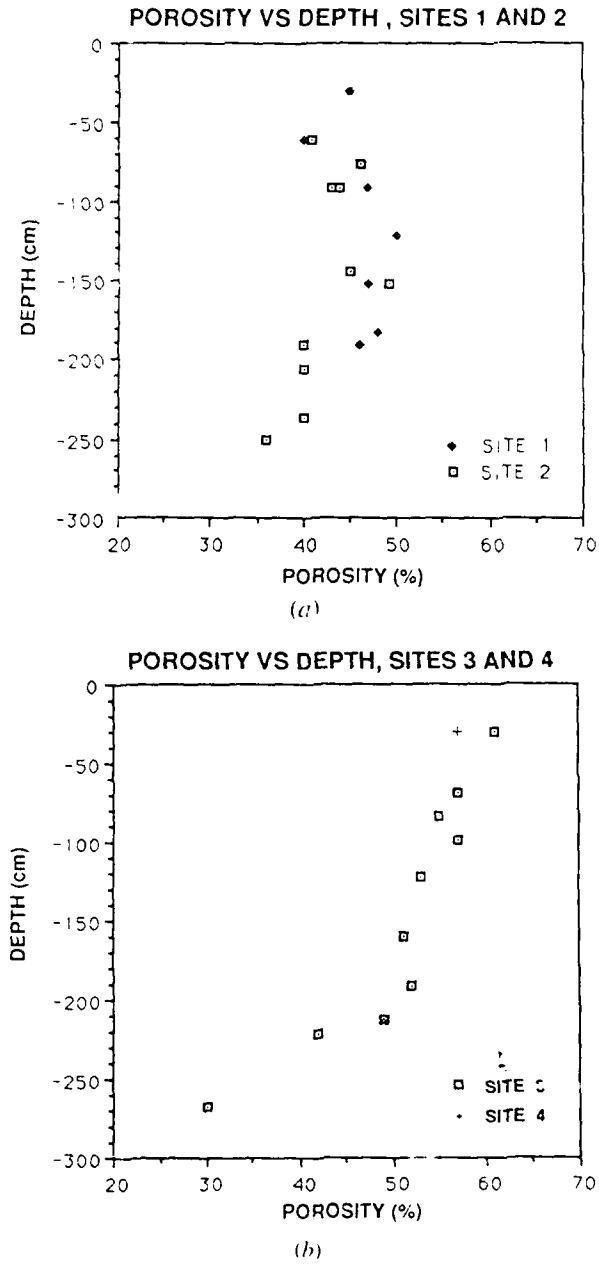

Figure 5. In situ porosity versus depth in sediment, (*a*) sites 1 and 2; (*b*) sites 3 and 4.

Whitman 1969); sandy marine sediments containing fines (>62.6 μm) have significantly different physical and mechanical properties compared to clean sands (Bennett and Nelsen 1983). The grain-supported Ottawa sand displays higher permeability and lower porosity than the matrix-supported oölitic sands. The fine-grained, aragonite-needle matrix clearly increases the porosity and substantially reduces the permeability of the material. Disturbance of clean sands would be expected to cause no change in permeability of samples tested at similar porosities. This was clearly evident by the agreement of data

from independent tests on Ottawa sand conducted by the current authors and by W. A. Dunlap (Texas A&M University, personal communication 1989).

Average grain density values ranged from 2.79 to 2.88 Mg/m^3 and averaged 2.84 Mg/m^3. These values are within the range of values between calcite (2.72 Mg/m^3) and aragonite (2.95 Mg/m^3). Close examination of the porosity, water content, and wet bulk density profiles (Figs. 5, 8, and 9) reveal that essentially no consolidation is apparent with depth of burial at site 1; however, some apparent consolidation is observed at site 2 below 150 cm subbottom. Sites 3 and 4 show the highest initial water contents and the greatest degree of apparent consolidation (Table 6). However, the decrease in porosity with depth of burial may be a function of the relative decrease in the percentage of fines. Examination of the upper 50 cm of sediment at sites 1 and 2 versus sites 3 and 4 reveals that a difference of approximately 10% in percentage of fines. A reduction in porosity

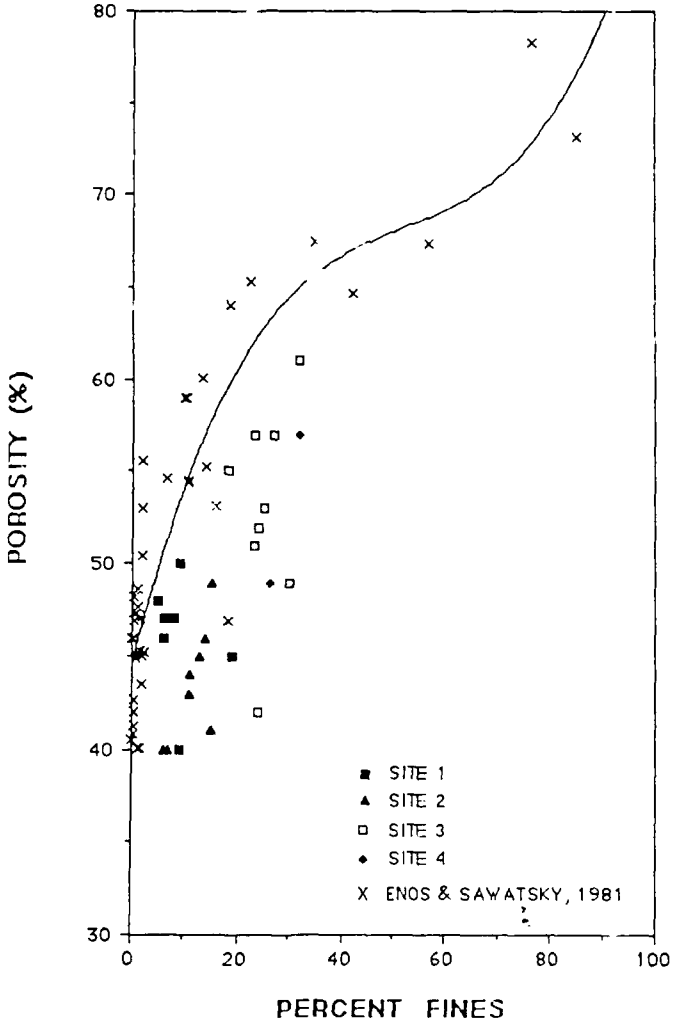

Figure 6. In situ porosity versus percent fines (particles less than 62.5 μm) for sites 1–4. Data by Enos and Sawatsky (1981) from laboratory determinations of porosity and percent fines is also plotted. The equation of the curve for the data by Enos and Sawatsky is $y = 44.595 + 1.1497x - 0.02x^2 + 0.0001285x^3$. The correlation coefficient, r, is 0.90.

Table 3
Sampling Description and Grain Size Data for Great Bahama Bank Samples Used for Laboratory Determinations of Porosity and Permeability

Site	Location	Water Depth (m)	Depth in Core (cm)	Grain Size (% by weight) Sand (2000–62.5 μm)	Silt (62.5–2 μm)	Clay (<2 μm)
1	25°15.8′N 78°50.5′W	5	182–187	94	1	3
3	25°22.2′N 78°56.4′W	4.7	24–29	57	29	13
			116–121	72	15	11
			207–212	75	14	9
			260–265	—	—	—
Ottawa sand				30–40 mesh, 425–600 μm		

from 61% to 42% is observed for site 3 within the upper 220 cm subbottom corresponding to an overburden stress, $\bar{\sigma}$, of only 17.5 kPa.

Site 2 sediments decrease in porosity from 44% to 36% within 250 cm subbottom (Table 2) with an effective overburden stress, $\bar{\sigma}$, of only 24.8 kPa, which is reasonable considering the low percentage of fines at this site. The higher porosities and greater decrease in porosity with burial depth at sites 3 and 4 compared to sites 1 and 2 are primarily a result of the much higher percent of fines present. Porosities at sites 1 and 2 are highest at about 150 cm subbottom and then decrease with depth of burial (Fig. 5), and this trend does not generally correlate with the percentage of fines (Fig. 4).

In situ permeabilities are plotted versus porosities and compared with data collected

Table 4
Laboratory-Measured Permeability and Porosity for Samples from Great Bahama Bank

Sample	Permeability K (darcy)	Permeability k (cm/s)	Porosity (%) Before[a]	Porosity (%) After[a]
Site 1, 182–187 cm	3.98	3.85×10^{-3}	39	46
Site 3, 24–29 cm	5.79	5.59×10^{-3}	54	60
Site 3, 207–212 cm	2.26	2.18×10^{-3}	50	49
Site 3, 260–265 cm	4.45	4.30×10^{-3}	47	41
Site 3, 24–29 cm (remolded)	1.99×10^{-2}	1.92×10^{-5}	62	—
Ottawa sand	207.0	0.20	36 38	—

[a] Porosity before and after permeability testing.

Table 5
In Situ Permeabilities, Great Bahama Bank

Summary	Depth (ft)	Depth (cm)	Permeability K (darcy)	Permeability k (cm/s)
Site 1	3	91	69	6.7×10^{-2}
	5	152	60	5.8×10^{-2}
	6	183	44	4.2×10^{-2}
	7.5	229	27	2.6×10^{-2}
	8.5	259	14	1.4×10^{-2}
Site 2	6.7	203	17	1.6×10^{-2}
	9	274	3	0.32×10^{-2}
Site 3	5.5	168	71	6.8×10^{-2}
	7	213	63	6.1×10^{-2}
	8.5	259	23	2.2×10^{-2}

Table 6
In Situ Water Content and Wet Bulk Density, Great Bahama Bank

	Depth (cm)	Water Content (%)	Wet Bulk Density (Mg/m^3)
Site 3A	84	45	1.8
	267	16	2.3
Site 3B	30	59	1.7
	69	50	1.8
	99	50	1.8
	122	35	1.9
	160	39	1.9
	191	40	1.9
	213	36	1.9
	221	27	2.1
Site 4	30	49	1.8
	213	35	1.9

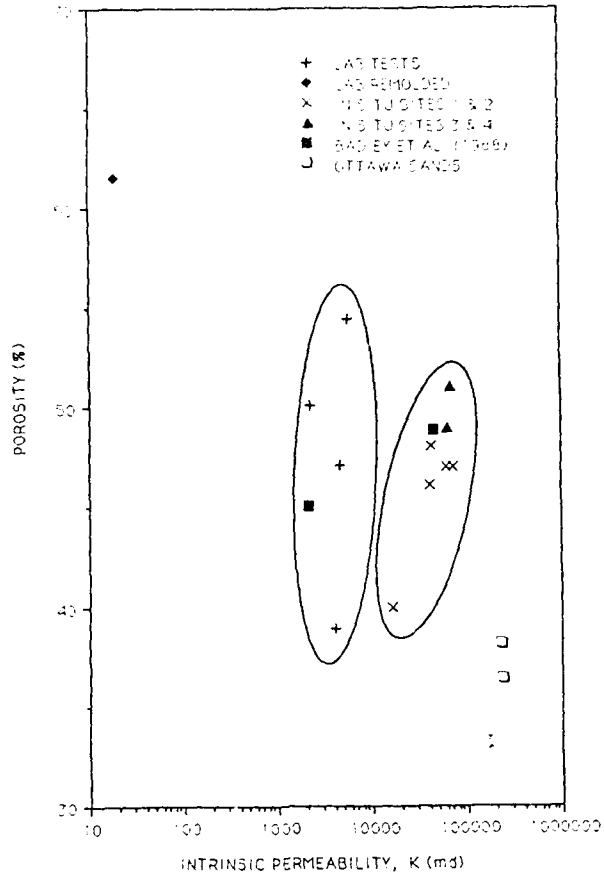

Figure 7. Plot of porosity versus permeability for oölitic carbonates from the Great Bahama Bank measured by in situ and laboratory techniques. Data from Badiey et al. (1988) are for laboratory measurements at atmospheric pressure in a variable-head permeability apparatus built by the Geo-Acoustics Laboratory of the University of Miami. Ovals delimit two major fields into which the data fall: (left) laboratory values; (right) in situ values.

from cores studied by Enos and Sawatsky (1981) from the Great Bahama Bank (Fig. 10). The in situ permeabilities fall among the highest values measured by Enos and Sawatsky on core samples. Although there is considerable scatter in the core data, a discernible trend in the Enos and Sawatsky data is observable; a decrease in permeability with increasing porosity, as was noted by Enos and Sawatsky. The data from Enos and Sawatsky was collected along a northwest transect from Andros Island to Browns Cay and consequently includes a broad range of environments. (This transect passes very near our sampling sites.) Although the in situ measurements are limited, our data indicate an increase in permeability with increasing porosity for sediments deposited in similar depositional environments. We suggest that the depositional porosity and permeability are largely controlled by both the grain size distribution and the microfabric. Both significantly influence pore size and geometry.

Enos and Sawatsky suggest that there was essentially no observable change in porosity with depth of burial to depths of at least 6.8 m. The in situ measurements of porosity (Table 2), the plots of water content and wet bulk density versus depth of burial (Figs. 8 and 9), and the in situ permeabilities (Table 5) reveal significant changes with

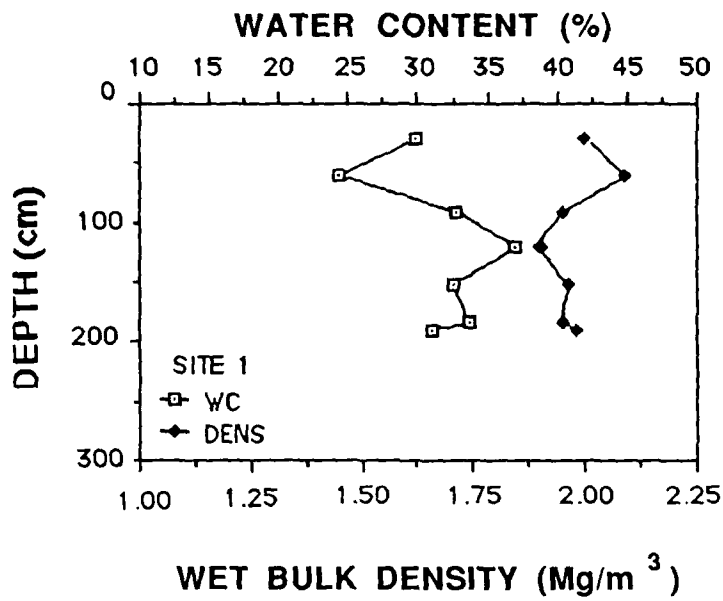

(*a*)

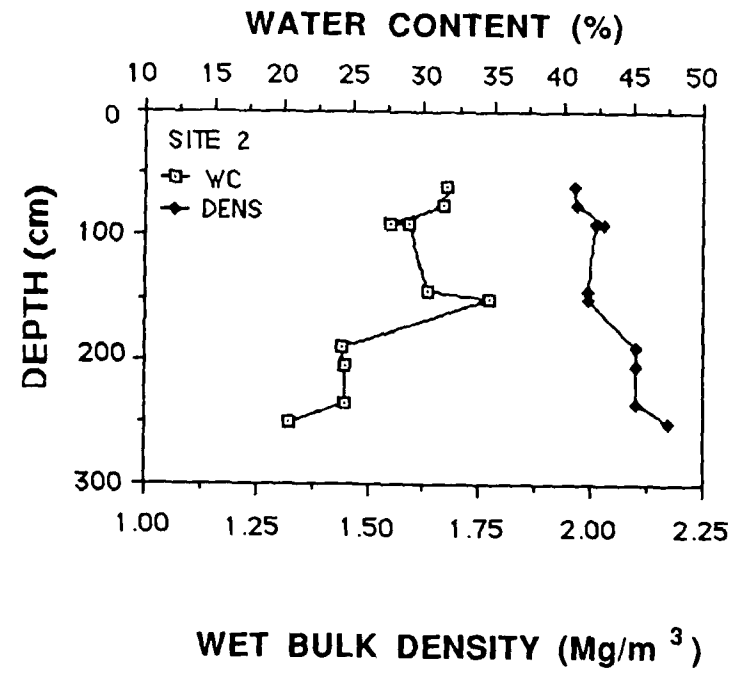

(*b*)

Figure 8. (*a*) Water content and wet bulk density calculated from in situ porosity and laboratory average grain density measurement plotted versus depth in sediment, site 1. (*b*) Water content and wet bulk density calculated as described in (*a*) plotted versus depth in sediment, site 2.

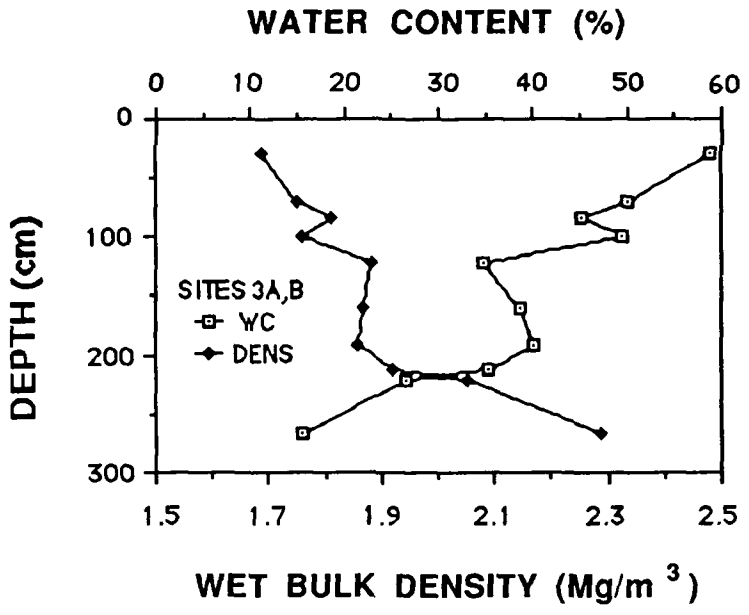

(*a*)

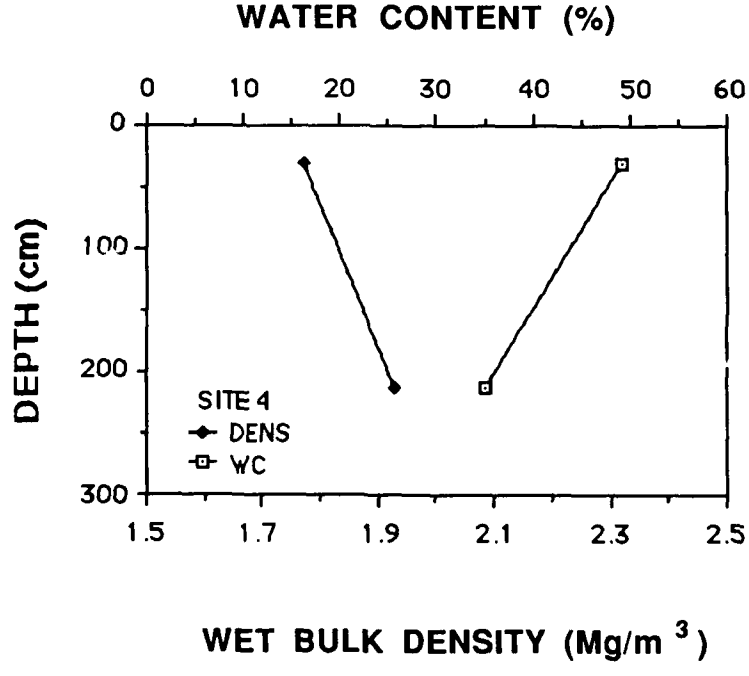

(*b*)

Figure 9. (*a*) Water content and wet bulk density calculated from in situ porosity and laboratory average grain density measurements plotted versus depth in sediment, sites 3A and 3B. (*b*) Water content and wet bulk density calculated as described in (*a*) plotted versus depth in sediment, site 4.

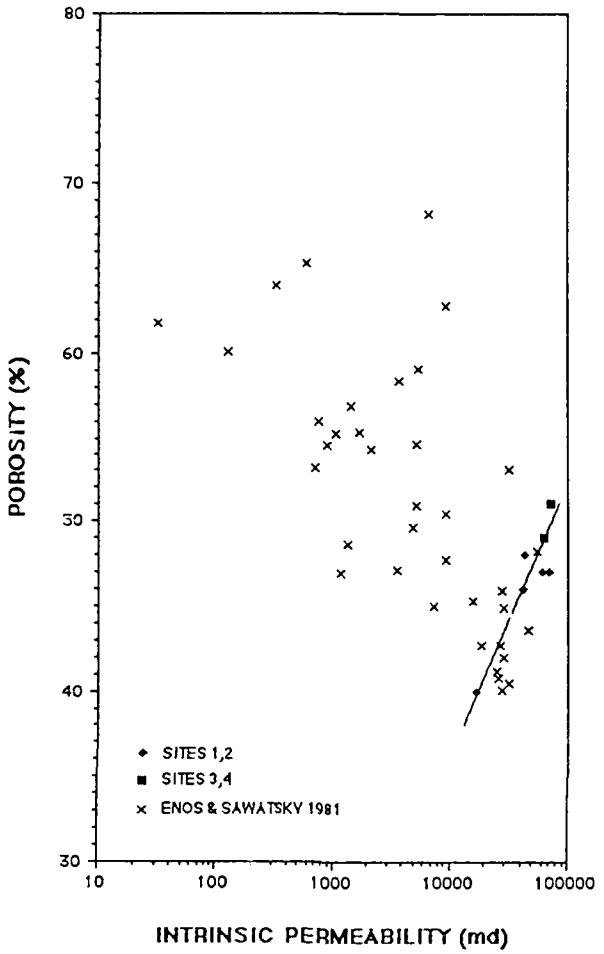

Figure 10. In situ porosity plotted versus in situ permeability for sites 1–4 (data connected by straight line). Core data from Enos and Sawatsky (1981) are also plotted.

depth of burial. Mechanical consolidation (dewatering) within the upper 2–3 m of these carbonate sediments is probably of lesser important. The greatest porosity reduction occurs in the carbonate sediments having the highest percentage of fines and is controlled largely by changes in the grain size distribution and in the absence of excess pore water pressures, the porosity and permeability decrease with decreasing pore size as depth of burial increases. It should be noted, however, that for deeply buried sediments less reduction in porosity has been observed for calcareous sediments than for terrigenous materials (Bryant et al., 1981).

Conclusions

In situ measurements of selected surficial shallow-water carbonate sediments revealed significant reduction in porosity and permeability with increasing depth of burial to subbottom depths of only 2.5 m. Sediment textures (grain size distribution) ranged from oölitic sands to aragonitic silty sands, and samples displayed a significant decrease in the percentage of fines with depth of burial. Although porosities were similar for both in situ

and laboratory tests, the in situ permeabilities were an order of magnitude higher than laboratory measurements. Coring and handling disturbance is considered the main cause of reduction in permeability results for laboratory measurements compared to in situ measurements.

Initial depositional porosities decrease from 61% to 42% at site 3 and from 44% to 36% at site 2. A major factor contributing to porosity reductions at these sites is the decrease in the percentage of fines with burial depth. Overburden stress is low (<25 kPa) at 2–2.5 m subbottom at these sites. These data, which are not in strict agreement with conclusions by Enos and Sawatsky (1981), indicate the following: (1) significant porosity reduction was observed with depth; (2) porosity decreased with a decrease in the percentage of fines; (3) permeability decreased with decreasing porosity; and (4) in situ permeabilities were an order of magnitude higher than laboratory values and were at the high end of the range of values measured by Enos and Sawatsky on core samples. Our results from a remolded sample suggest that coring in noncohesive or weakly cohesive granular carbonate sediments which contain a fine-grained matrix causes severe distortion and disturbance of dewatering pathways and particle rearrangements. This has been well known by the geotechnical engineering profession for many years and is a primary reason for the lack of reliable physical property data for noncohesive sediments. The depositional porosities of 45% measured in situ for the sites 1 and 2 oölitic sands are in close agreement with initial porosities estimated for the oölitic Miami limestone of the lower Florida Keys (Schmoker and Hester 1986).

Significant variability, laterally and vertically, was observed in the selected physical properties of these carbonate sediments. Caution should be exercised when estimates of physical properties are applied to acoustic models and geotechnical engineering problems, particularly when only limited sources of sediment data are available. Grain size data alone are insufficient for predicting the porosities and permeabilities of weakly cohesive sands containing a fine-grained matrix. We suggest that these parameters are largely controlled by the microfabric and gram size distribution, the environmental processes, and specifically the consolidation history. At high overburden stress, compaction processes that drive out the interstitial water alter the particle arrangements (microfabric) and change the pore size distribution, thus changing the porosity and permeability (Bennett et al. 1989).

Acknowledgments

This project was sponsored by the Office of Naval Research Contract Research Program (Joseph Kravitz) and the Naval Ocean Research and Development Activity. The authors appreciate the critical reviews of a draft version of this manuscript by Richard Rezak, Philip Valent, Dawn Lavoie, and Patti Burkett. We appreciate the critical reviews and helpful suggestions of Henry Mullins and Jeff Dravis, which have improved the quality of the final manuscript. E. Shinn, U.S. Geological Survey, Miami, assisted in field site selection.

We thank Lee Nastav for preparing the figures and for editorial suggestions. The authors especially acknowledge the efforts of David Young in building the vibrocoring system and laboratory permeability apparatus and in various pre-cruise assignments. The authors are indebted to the late John T. Burns for his field assistance and instrumentation development efforts. Kathleen Fischer was funded by the National Research Council-NORDA Research Associateship Program.

References

Archie, G. E. 1942. The electrical resistivity log as an aid in determining some reservoir characteristics. *American Institute of Mechanical Engineering* 146:54–61.

Badiey, M., T. Yamamoto, A. Turgut, R. Bennett, and C. S. Conner. 1988. Laboratory and in situ measurements of selected geoacoustic properties of carbonate sediments. *Journal of the Acoustical Society of America* 84:689-696.

Bennett, R. H., and M. H. Hulbert. 1986. *Clary microstructure.* Boston: International Human Resources Development Corporation Press (now distributed by Prentice Hall, Englewood Cliffs, NJ).

Bennett, R. H., and T. A. Nelsen. 1983. Seafloor characteristics and dynamics affecting geotechnical properties at shelfbreaks. In *The shelfbreak: Critical interface on continental margins,* ed. D. J. Stanley and G. T. Moore. Society of Economic Paleontologists and Mineralogists Special Pub. no. 33. Tulsa, OK.

Bennett, R. H., D. N. Lambert, M. H. Hulbert, J. T. Burns, W. B. Swayer, and G. L. Freeland. 1983. Electrical resistivity/conductivity in seabed sediments. In *CRC handbook of geophysical exploration at sea,* ed. R. A. Geyer. Boca Raton, FL: CRC Press.

Bennett, R. H., K. Fischer, Huon Li, R. Baerwald, M. H. Hulbert, T. Yamamoto, and M. Badiey. 1990. In situ porosity and permeability of selected carbonate sediment: Great Bahama Bank. Part 2: Microfabric. *Marine Geotechnology* 9:29–42.

Bennett, R. H., K. M. Fischer, D. L. Lavoie, W. R. Bryant, and R. Rezak. 1989. Porometry and fabric of marine clay and carbonate sediments: Determinants of permeability. *Marine Geology* 89:127–152.

Bhattacharyya, A., and G. M. Friedman. 1984. Experimental compaction of oöids under deep-burial diagenetic temperatures and pressures. *Journal of Sedimentary Petrology* 54:362–372.

Bryant, W. R., W. Hottman, and P. Trabant. 1974. Permeability of unconsolidated and consolidated marine sediments, Gulf of Mexico. Report, Texas A&M University, College of Geoscience (January).

Bryant, W. R., R. H. Bennett, and C. Katherman. 1981. Shear strength, consolidation, porosity, and permeability of oceanic sediments. In *The oceanic lithosphere, Vol. VII: The sea,* ed. C. Emiliani. New York: Wiley-Interscience.

Connor, C. S. 1986. Field measurements of water wave pressure and seabed velocity near the seabed surface. M.S. thesis, University of Miami, Coral Gables, FL.

Dakhnov, V. N. 1962. Geophysical well logging. *Quarterly of the Colorado School of Mines* 57.

Dunham, R. J. 1962. Classification of carbonate rocks according to depositional texture. In *Classification of carbonate rocks, a symposium,* ed. W. E. Ham. American Association of Petroleum Geologists Memoir 1.

Eckert, E. R. G., and R. M. Drake. 1972. *Analysis of heat and mass transfer.* New York: McGraw-Hill.

Enos, P., and L. H. Sawatsky. 1981. Pore networks in Holocene carbonate sediments. *Journal of Sedimentary Petrology* 51:961–985.

Erchul, R. A. 1974. Ocean engineering applications for electrical resistivity techniques. *Offshore Technology Conference.*

Evans, C. C., and R. N. Ginsburg. 1987. Fabric-selective diagenesis in late Pleistocene Miami Limestone. *Journal of Sedimentary Petrology* 57:311–318.

Fischer, K. M., H. Li, R. H. Bennett, and W. A. Dunlap. 1990. Calculation of permeability coefficients of soils and marine sediments. *Environmental Software* 5:29–37.

Ginsburg, R. N., R. M. Lloyd, K. W. Stockman, and J. S. McCallum. 1963. Shallow-water carbonate sediments. In *The sea, Vol. 3.,* ed. M. N. Hill. New York: Interscience.

Hulbert, M. H., D. N. Lambert, R. H. Bennett, G. L. Freeland, J. T. Burns, and W. B. Sawyer. 1981. Electrical resistivity/conductivity of submarine sediments measured by in situ techniques. *NOAA Technical Report ERL 416-AOML 31.* Washington, D.C.: U.S. Department of Commerce.

Illing, L. V. 1954. Bahaman calcareous sands. *American Association of Petroleum Geologists Bulletin* 38:1-95.

Imbrie, J., and Purdy, E. G. 1962. Classification of modern bahamian carbonate sediments. In *Classification of carbonate rocks*, ed. W. E. Ham. Tulsa, Okla.: American Association of Petroleum Geologists.

Lambe, T. W. 1951. *Soil testing for engineers*. New York: Wiley.

Lambe, T. W., and R. V. Whitman. 1969. *Soil mechanics*. New York: Wiley.

Lambert, D. N., F. S. Carnaggio, and P. J. Valent. 1986. A self-contained diver operated conductivity/resistivity probe. *Current Practices and New Technology in Ocean Engineering* 11:385-393.

Li, H., and R. H. Bennett. In press. Significance of sediment-flow dynamics on clay microstructure development: Riverine and continental shelf environments. In *Microstructure of fine grained sediments: from mud to shale*, ed. R. H. Bennett, M. H. Hulbert, and W. R. Bryant. New York: Springer-Verlag.

Lowe, J., III, P. F. Zaccheo, and H. S. Feldman. 1964. Consolidation testing with pack pressure. *Journal of the Soil Mechanics and Proceedings, American Society of Civil Engineers* 90:69-86.

Morelock, J., and W. R. Bryant. 1972. Consolidation of marine sediments. In *Contributions on geology and geophysics, and oceanography of the Gulf of Mexico: TAMU oceanography studies 3*, ed. B. J. Henry and R. Rezak. College Station: Texas A&M University.

Mullins, H. T., and C. Neumann. 1979. Geology of the Miami Terrace and its paleo-oceanographic implications. *Marine Geology* 30:205-232.

Purdy, E. G. 1963a. Recent calcium carbonate facies of the Great Bahama Bank. 1. Petrography and reaction groups. *Journal of Geology* 71:334-355.

Purdy, E. G. 1963b. Recent calcium carbonate facies of the Great Bahama Bank. 2. Sedimentary facies. *Journal of Geology* 71:472-497.

Richards, A. F. 1962. Investigations of deep-sea sediment cores, II. Mass Physical properties. Technical Report, TR-106. Washington, D.C.: U.S. Hydrographic Office.

Schmoker, J. W., and T. C. Hester. 1986. Porosity of the Miami Limestone (late Pleistocene), lower Florida Keys. *Journal of Sedimentary Petrology* 56:629-634.

Shinn, E. A., R. M. Lloyd, and R. M. Ginsburg. 1969. Anatomy of a modern carbonate tidal-flat, Andros Island, Bahamas. *Journal of Sedimentary Petrology* 39:1202-1228.

Yamamoto, T., and R. H. Bennett. 1986. Laboratory measurements of selected geo-acoustic properties of carbonate sediments at the Great Bahama Bank (abst.). *Journal of the Acoustical Society of America* Suppl. 1, 79:S41.

Appendix A: Resistivity-Porosity

In situ measurement of sediment electrical conductivity (the reciprocal of resistivity) provides a means of determining the porosity and wet bulk density of seafloor deposits of cohesive materials and noncohesive sands and gravels (Bennett et al. 1983). With present technology, noncohesive sediments are virtually impossible to recover in an undisturbed condition and are generally not suitable for measurement of geotechnical and geoacoustic properties by laboratory techniques. (For this reason, most of the early literature data for the physical properties of the Great Bahama Bank sediments are highly suspect.) The system and probes used in this project are similar to those described earlier by Hulbert et al. (1981) and Bennett et al. (1983). One major difference, however, is that a probe tip having a considerably smaller diameter (5.5 cm) could penetrate the oölitic sands found in the Great Bahama Bank, compared to the very robust tip design (12.5 cm) required to penetrate the coarse carbonates and reefal debris off the Florida Shelf.

The conductivity probe uses the four-electrode contact technique consisting of two pairs of electrodes, one pair for applying the reference current and the other for measuring the resulting electrical potential (Fig. A-1). Details of the systems and in situ porosity data for coarse-grained carbonates off the Florida Shelf can be found elsewhere (Hulbert et al. 1981; Bennett et al. 1983). The small probe tip design used during this study has been thoroughly described by Lambert et al. (1986).

The porosity, n, of a sedimentary deposit is related to the formation of resistivity factor or formation factor, F, as given by Archie (1942):

$$F = n^{-m} \tag{A-1}$$

which was later modified by Dakhnov (1962) as follows:

$$F = an^{-m} \tag{A-2}$$

where a is a factor of proportionality that depends on the ratios of the fine fractions ($<$ 62.5 μm) to the coarse fraction ($>$62.5 μm) of the sediment of interest. The exponent, m, is usually called the shape factor (Lambert et al., 1986). Coefficients for Eq. (A-2) have been reported for several sediment types by Erchul (1974). For sands, Erchul determined values of 1.4 to 1.6 for the coefficient a and 1.0 to 1.1 for the exponent m. In this study values for a and m were found to be as follows:

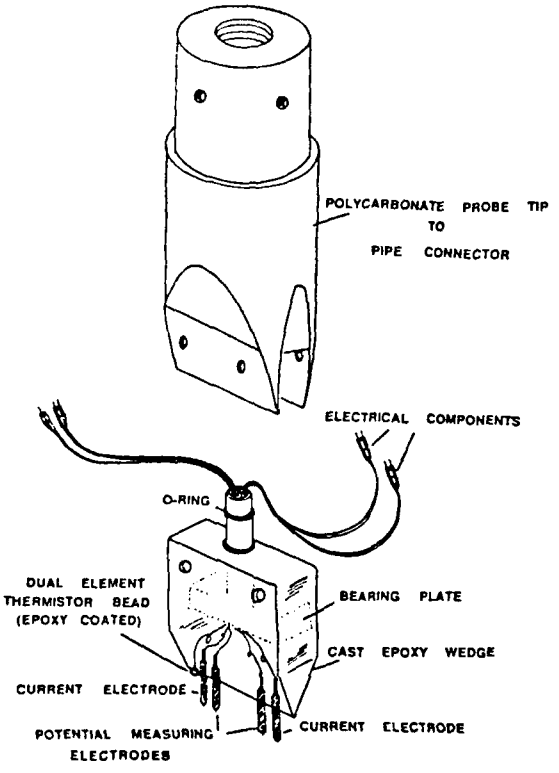

Figure A-1. Component sketch of in situ conductivity probe tip and mounting connector.

a = 1.27 and m = 1.11 for sites 1 and 2 (oölitic sand)
a = 1.48 and m = 1.11 for sites 3 and 4 (muddy oölitic sand)

The relationship between porosity and resistivity is valid for sediments composed of solid particles and would not be expected to apply directly for sediments composed of particles having significant intraparticle porosity such as foram oozes.

Techniques for calibration of the conductivity system and probe tip are described in detail by Hulbert et al. (1981), Bennett et al. (1983), and Lambert et al. (1986).

Appendix B: In Situ Permeability

Permeability measurements were accomplished through use of a falling-head permeameter. In our application of this technique, a probe that contains a porous segment is emplaced vertically in the sediment. An initial hydrostatic head is established at the porous element via a vertical column of water. The subsequent rate of decay of the pressure head as water flows through the porous element into the surrounding sediment can be related, through Darcy's law, to the permeability of the sediment.

The important components of the permeability probe are illustrated in Figure B-1. The probe consists of a cylindrical porous stone positioned between a pipe and a solid, conical tip. The porous stone is supported internally by a perforated pipe. The length of the porous stone is 9.9 cm, and the inside and outside diameters are 3.25 and 4.25 cm, respectively. The entire assembly is attached to the vibrocorer driving head. A flexible hose connects the top of the probe assembly with a 25.27-liter water reservoir located on the deck of the vessel. The reservoir is calibrated so that the volumetric flow associated with a decrease in pressure head can be determined. The arrangement of the various components is shown schematically in Figure B-2.

Modeling of in Situ Permeability Probe

For purposes of analysis, it is assumed that the porous stone can be represented by an isolated, porous sphere of diameter d with the center located a depth D below the sediment-water interface of a semi-infinite porous medium (Fig. B-3). If a slowly varying differential pressure head $h(t)$ is maintained at the surface of the sphere, then the instantaneous volumetric flow $Q(t)$ into the sediment is given by

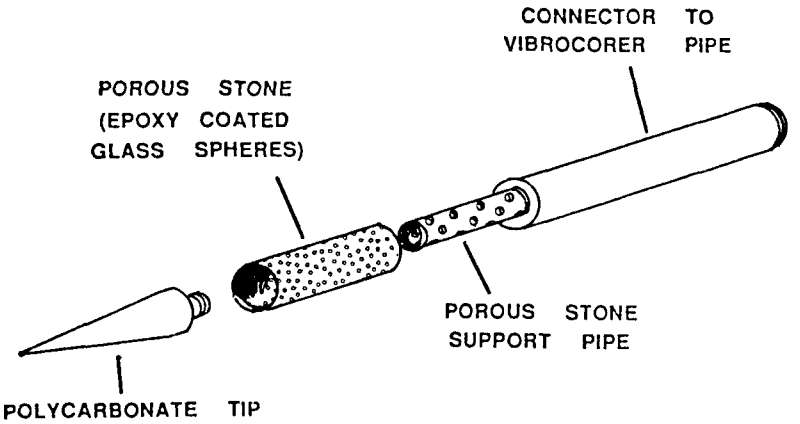

Figure B-1. Component sketch of in situ permeability probe.

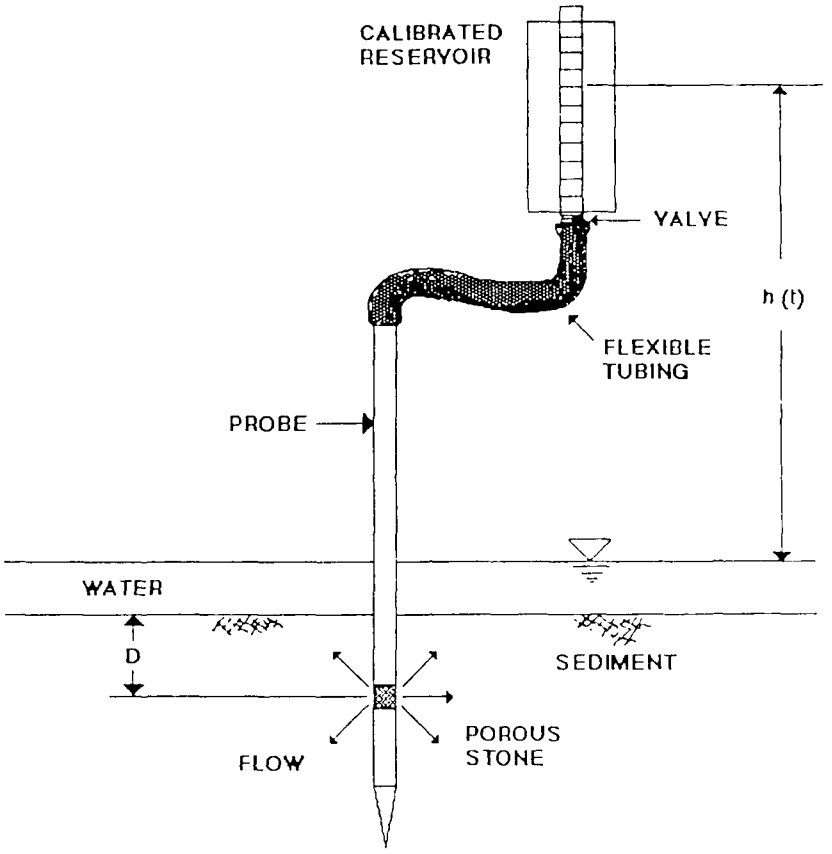

Figure B-2. Generalized scheme for in situ permeability measurement (not drawn to scale).

$$Q(t) = \frac{2\pi\, dK\rho g}{\mu(1 - d/4D)}\, h(t) \tag{B-1}$$

where K is the intrinsic, or sediment, permeability, μ is the dynamic viscosity of the saturating fluid, ρ is the fluid density, and g is the acceleration of gravity. The above result is obtained by direct analogy with the case of steady heat conduction from an isothermal sphere embedded in a semi-infinite medium with a surface maintained at a temperature different from that of the sphere (Eckert and Drake 1972, p. 106). To apply Eq. (B-1), the surface area of the sphere is set equal to the external surface area A of the cylindrical porous stone. The sphere diameter is then

$$d = \sqrt{\frac{A}{\pi}} \tag{B-2}$$

The modeling of the permeameter response by Eqs. (B-1) and (B-2) embodies the assumption that near-field effects are of minor importance in determining the overall flow rate, and hence it is not necessary to use the exact geometry of the porous stone. Conservation of mass requires that the volumetric flow rate $Q(t)$ be related to the pressure head dh/dt by

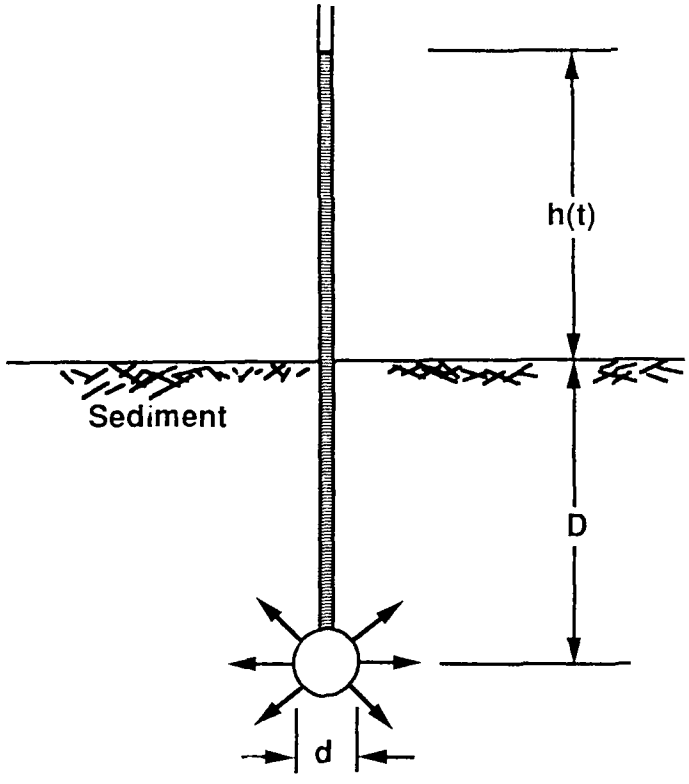

Figure B-3. Geometry used to model the in situ permeability probe.

$$Q(t) = -b\frac{dh}{dt} \tag{B-3}$$

where b is the cross-sectional area of the reservoir where the head change is measured. Combination of Eqs. (B-1) through (B-3) then provides

$$\frac{dh}{dt} = -Ch(t) \tag{B-4}$$

where

$$C = \frac{2\pi\, dK\rho g}{b\mu(1 - d/4D)} \tag{B-5}$$

In the expression for C, the quantity $Kg\rho/\mu$ is usually referred to as Darcy's coefficient of permeability, k, which has units of cm/s. The intrinsic permeability, K, which has units of cm^2, is a measure of the permeability of a sediment, which is independent of the fluid properties. The darcy is a common unit of permeability, and 1 darcy has the value of 9.89×10^{-9} cm^2. For a constant C, integration of Eq. (B-4) provides

$$h(t) = h_0 \exp(-Ct) \tag{B-6}$$

where h_0 is the initial differential head and t is the elapsed time.

The sediment permeability can be inferred using either of two approaches. In the first method, C can be determined from a curve fit of h versus t based on Eq. (B-6), and the permeability then obtained from Eq. (B-5). A second method is based on the integration of Eq. (B-4) over a time interval Δt between elevation heads h_1 and h_2, yielding

$$C = -\frac{1}{\Delta t} \ln\left(\frac{h_2}{h_1}\right) \tag{B-7}$$

Knowing C, the intrinsic permeability K is, as before, obtained from Eq. (B-5).

Prior to its use, the permeameter must be calibrated to properly account for the intrinsic head loss associated with flow through the system consisting of the reservoir, valve, tubing, pipe, and porous stone. This is accomplished by establishing flow through the permeameter while immersed in water. The intrinsic permeability of the instrument, K_i, is then determined from measurements of the head loss characteristics, as described in the previous paragraph. Given the approximate nature of the analysis, it is appropriate to calibrate the instrument using a material of known permeability in order to obtain improved accuracy.

The in situ application of the permeameter provides a measurement of an apparent permeability, K_{app}, resulting from the combined flow resistance of the sediment and the permeameter itself. From Eq. (B-1), it is clear that the volumetric flow rate from the porous sphere is given by $Q = (l_\infty K_\infty/\mu)\,\Delta p_\infty$, where l_∞ is a length, K_∞ is the sediment permeability, and Δp_∞ is the pressure difference which exists between the surface of the porous sphere and the far field. The volumetric-flow-rate/pressure-loss characteristics of the permeameter itself can be represented by $Q = (l_i K_i/\mu)\,\Delta p_i$, for slow viscous flow through the system, where K_i is the intrinsic permeability of the instrument, Δp_i is the pressure drop, and l_i is a length. In the in situ application of the permeameter, the pressure drops Δp_∞ and Δp_i act in series to produce an overall pressure loss Δp. The response of the permeameter can then be represented in terms of the overall pressure drop $\Delta p = \Delta p_\infty(1 + \Delta p_i/\Delta p_\infty)$ by $Q = (l_\infty K_{app}/\mu)\,\Delta p$, where the apparent permeability K_{app} is given by

$$K_{app} = \frac{K_\infty}{1 + (l_\infty K_\infty/l_i K_i)} \tag{B-8}$$

In typical applications, $l_\infty K_\infty/l_i K_i \ll 1$, $\Delta p_i/\Delta p_\infty \ll 1$, and $d \ll D$, resulting in obvious simplifications to Eqs. (B-5) and (B-8). In particular, Eq. (B-8) yields $K_\infty \approx K_{app}$, and the apparent permeability measured with the permeameter is essentially equal to the sediment permeability. Typical values for the parameters used in the current investigation are $d = 6.5$ cm, $A = 132.2$ cm^2, $D = 91$–274 cm, and $K_i = 3.8 \times 10^{-5}$ cm^2.

Appendix C: Laboratory Permeability

A specially designed, back pressure permeameter was built to measure the permeability of coarse-grained, porous sediment (quartz and carbonates) characterized by high flow rates, i.e., having coefficients of permeability as high as $K = 1.0$ darcy. The purpose of permeability testing with applied back-pressure is to ensure saturation of the sediment

sample in much the same way as employed in back-pressure consolidometers (Lowe et al. 1964; Bryant et al. 1974). Saturation of the sample is necessary since free air bubbles seriously reduce fluid flow in porous media.

The permeability apparatus, shown in Figure C-1, consists of two clear plastic tubes (7.5-cm ID, 8.9-cm OD) connected by a large, high-pressure ball valve with appropriate plumbing. The system is connected to a 689-kPa (100-psi) air source. Sample compartment G is installed in the base of standpipe E. With ball valve H closed, water is added to the standpipe by removing the upper section of the pressure equalization tube D. The system is sealed by reinserting tube section D and closing both drain valves (K and L). Safety shields cover E, H, and J, and a safety clamp is attached to tube D. Valve H is opened to initiate fluid flow, and the system is pressurized to 689 kPa by turning valve C to the pressure position and opening valve A. Valve A is closed when gauge B reads 689 kPa. Water levels are recorded from scale F, and corresponding times are noted. Water collecting in reservoir J is not allowed to exceed the level of the base of umbrella I. (Umbrella I covers the end of the pressure equalization tube D, which ensures uniform pressure throughout the system.) At the end of the test, water is drained from reservoir J by opening valve K. When all water has drained from reservoir J, valve L is opened and valve C is switched to the vent position.

Our permeability apparatus is based on the standard variable-head test. The Darcy's coefficient of permeability can be calculated from the following equation (Lambe 1951):

$$k = \frac{2.3aL \log_{10}(h_0/h_1}{A(t_1 - t_0)} \tag{C-1}$$

where a = cross-sectional area of the standpipe
A = cross-sectional area of the sediment sample
L = length of sediment sample
t_0 = time when water in the standpipe is at h_0
t_1 = time when water in the standpipe is at h_1
h_0, h_1 = water levels, as measured from the bottom of the sediment sample (Fig. C-1)

Darcy's coefficient of permeability is converted to intrinsic permeability K, that is, the permeability of the sediment independent of the fluid properties, by the equation

$$K = \frac{k\mu}{\rho g} \tag{C-2}$$

where ρ is the fluid density, g is the acceleration due to gravity, and μ is the dynamic viscosity of the fluid. K is often expressed in units of darcys, where 1 darcy has the value of 9.89×10^{-9} cm^2.

Samples of Ottawa sands (30–40 mesh) were used for the initial testing of the permeability apparatus at 689 kPa. The results are very consistent (k, average = 0.20 cm/s, that is, K = 207 darcys; standard deviation, σ = 0.02 cm/s; n = 18; Fischer et al. 1990) and agree very well with earlier independent measurements of the same material (Dunlap, Texas A&M University, personal communication 1988). Consistent results also were obtained for Ottawa sands at atmospheric pressure.

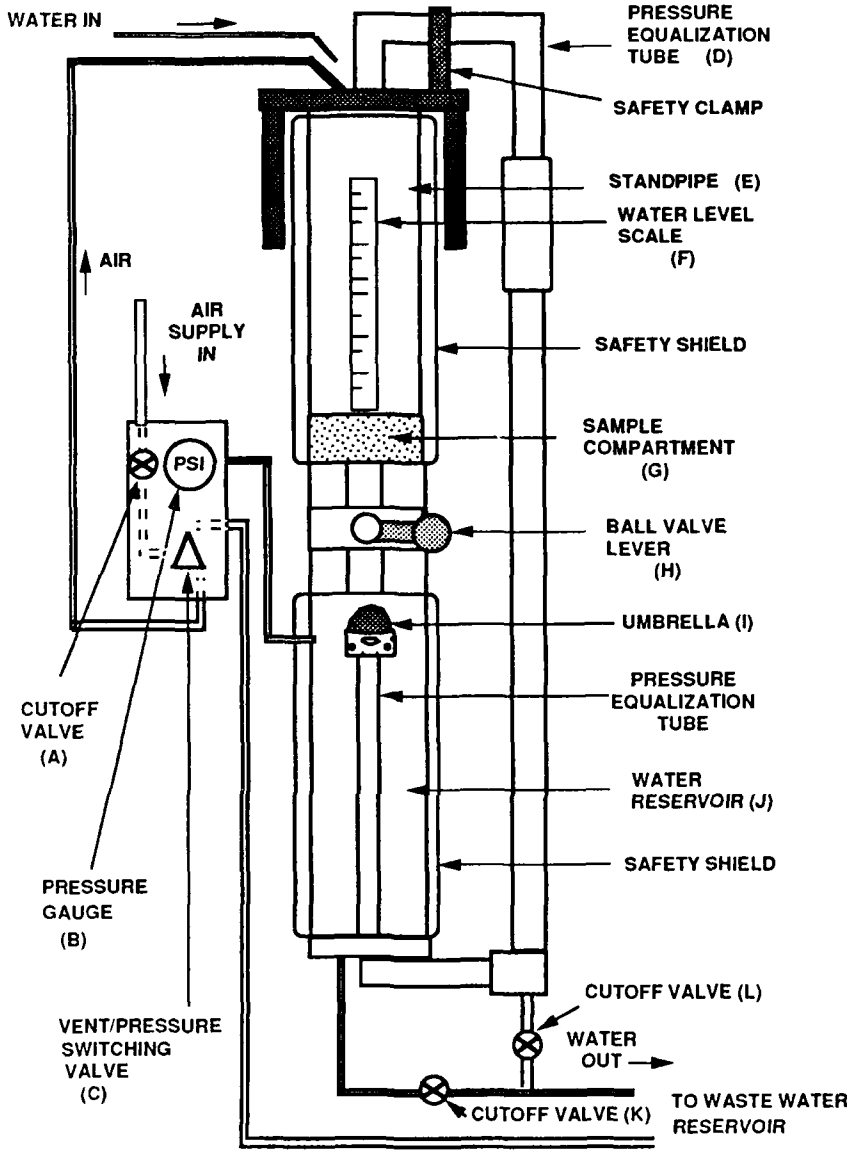

Figure C-1. (*a*) Schematic drawing of the variable-head permeability apparatus used in this study. The system is designed to apply safely a back-pressure of 689 kPa. Major components are labeled.

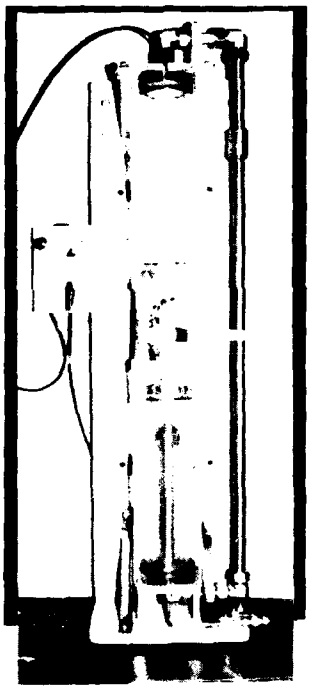

Figure C-1. (*Continued*) (*b*) Photograph of apparatus.